2205 双相不锈钢焊接热影响区的组织转变行为

熊庆人[1]， 霍春勇[1]， 李为卫[1]， 张建勋[2]
（1. 中国石油天然气集团公司 管材研究所，西安 710065；
2. 西安交通大学 材料科学与工程学院，西安 710049）

摘 要：通过焊接热模拟方法和现代材料组织分析技术，研究了冷却时间 $t_{8/5}$ 和 $t_{12/8}$ 对 2205 双相不锈钢模拟热影响区（HAZ）组织转变行为的影响。结果表明，固定 $t_{12/8}$，改变 $t_{8/5}$，2205 双相不锈钢模拟 HAZ 的组织形态和相比例相差不大，用 $t_{8/5}$ 作为参数研究这种材料 HAZ 组织转变行为是不恰当的；固定 $t_{8/5}$，改变 $t_{12/8}$，2205 双相不锈钢模拟 HAZ 的组织形态和相比例变化比较大，$t_{12/8}$ 是影响这种材料 HAZ 组织的本质因素，用它来研究对 2205 双相不锈钢 HAZ 组织的影响更为确切。冷却时间 $t_{12/8}$ 对 2205 双相不锈钢模拟 HAZ 组织的影响规律是，随着 $t_{12/8}$ 的增加，奥氏体由原来的长条状逐渐变成树枝状，晶界和晶粒内部均析出奥氏体，相互交集在一起形成网状。铁素体的比例随着冷却时间 $t_{12/8}$ 的增加而缓慢下降；2205 双相不锈钢模拟 HAZ 组织中奥氏体和铁素体晶内比母材有更多的位错。

关键词：双相不锈钢；热影响区；组织；相比例
中图分类号：TG457.1 文献标识码：A 文章编号：0253－360X（2007）11－053－05

熊庆人

0 序 言

2205 双相不锈钢是第二代双相不锈钢的典型代表，具有优异的力学性能和耐腐蚀性能，广泛用于运输、石油、天然气、海洋和化工等行业。自从 20 世纪 30 年代早期双相不锈钢发明以来，该材料的焊接一直是比较关注的课题。现代的双相不锈钢由于采用氮合金化等技术，焊接性能有很大改善，但与普通奥氏体不锈钢焊接相比还是有许多问题，被公认为是难焊接的材料[1,2]。从国内外的研究来看，2205 双相不锈钢在焊接过程中，最为突出的问题也是热循环对焊接接头微观组织及其塑韧性和抗腐蚀性的影响[3]。焊接热影响区是焊接接头的薄弱区域，焊接工艺参数对该区域的组织和两相比例有很大影响，而组织和相比例的变化会对材料的力学性能和耐腐蚀性能产生很大影响。而这一区域非常狭小，用常规的焊接试验方法难以对该区域的组织和性能进行准确试验评价，焊接热模拟试验为研究该区域的组织性能提供了良好的手段。

收稿日期：2007－04－09
基金项目：中国石油天然气集团公司科学研究与技术开发资助项目（04B41101）

焊接热循环的特性是由四个主要参数组成[4]：加热速度 ω_H、峰值温度 T_p、高温持续时间 t_H 和某一温度区间的冷却时间 t_A。关于冷却时间，对于一般碳钢或低合金钢材料，人们关注的是从 800～500 ℃的冷却时间 $t_{8/5}$，这是因为 800～500 ℃是奥氏体最不稳定的温度范围，$t_{8/5}$ 的长短将决定该材料最终的相变产物。而 2205 双相不锈钢属于高合金钢，其相图与一般碳钢和低合金钢 Fe－C 合金相图有很大的区别，用 $t_{8/5}$ 来研究 2205 双相不锈钢焊接性是否恰当，用哪个区间的冷却时间研究更为合适，模拟焊接热影响区的组织如何随冷却时间转变，以下进行了较深入的探讨。

1 试 验

试验用 2205 双相不锈钢板材厚度为 12.7 mm，由芬兰 Outokumpu 公司提供，其主要化学成分（质量分数，%）为：C 0.017，Si 0.41，Mn 1.40，Cr 22.83，Ni 5.66，Mo 3.4，N 0.18。材料为固溶处理状态，其力学性能抗拉强度为 680 MPa，屈服强度为 480 MPa，断后伸长率 A 为 25%，－20 ℃夏比冲击吸收功 A_{KV} 为 150 J。图 1 为 2205 双相不锈钢原始母材的金相组织照片，由铁素体和奥氏体两相组成，奥氏体被基

体铁素体组织包围着，并且大部分晶粒呈现条带状。组织中也有一些细碎条状的奥氏体，弥散分布在铁素体中。具有体积分数大体相等的特征（铁素体约占55%）。

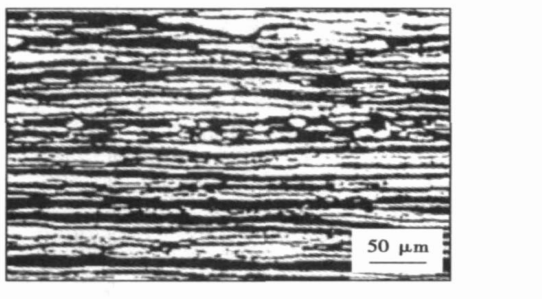

图 1 2205 双相不锈钢母材组织

Fig. 1 Microstructure of 2205 duplex stainless steel base metal

在板材上沿横向取样加工热模拟试样，试样尺寸为12 mm×12 mm×80 mm。焊接热循环曲线根据式(1)[5]所示的方程计算。研究表明，式(1)可以在热模拟中很好地反映焊接过程的热循环。焊接热模拟循环参数加热速度、峰值温度和高温停留时间见表1，冷却时间在下文述及。

$$T-T_0=\sqrt{\frac{t_{8/5}(500-T_0)^2(800-T_0)^2}{300(1\,300-2T_0)t}}\times \exp\left[\frac{-t_{8/5}(500-T_0)^2(800-T_0)^2}{2e(300)(1\,300-2T_0)(T_{max}-T_0)^2t}\right], \quad (1)$$

式中：T 为实际温度；T_0 为预热温度或层间温度；T_{max} 为最高加热温度；$t_{8/5}$ 为800 ~ 500 ℃的冷却时间；t 为时间。

表 1 焊接热模拟试验参数表

Table 1 Parameter of thermal simulation test

加热速度 ω_H/(℃·s^{-1})	峰值温度 T_{max}/℃	高温停留时间 t_H/s
200	1 300	1

采用 DM — 100A 型热模拟机进行热模拟试验。热模拟试验后，对试样横截面进行光学金相检验（型号为MeF3 ROTOSCOPE）和透射电镜（型号为 JEM — 200CX）分析。金相组织浸蚀方法为：以铁氰化钾碱性试液30 gKOH＋30 g$K_3Fe(CN)_6$＋100 mL H_2O 在温度90 ~ 95 ℃下进行化学浸蚀，时间约为 3 min。采用Photoshop 软件对金相照片进行处理，分离出铁素体和奥氏体，计算出在不同热模拟参数下组织中两相的比例。每个试样取 5 ~ 6 张图像算出相比例（面积百分比），然后求平均值。

2 结果与讨论

2.1 初步的试验结果及分析

选取不同焊接热输入参数下的冷却参数，取 $t_{8/5}$ 分别为 7，20，50 和100 s，相应的 $t_{12/8}$ 分别为 3.6，7，18 和37 s。图2 是不同 $t_{8/5}$ 下模拟HAZ 的组织形态。

当 $t_{8/5}$＝7 s时（图 2a），从组织形态上看，组织的大体形态和母材组织相似，但奥氏体的量比母材明显减少，铁素体相比例与母材相比明显高；当 $t_{8/5}$＝20 s时（图 2b），组织形态发生了较大变化，粗大的铁素体晶粒边界和晶粒内部均析出了羽毛状和树枝状的奥氏体相，铁素体相比例约为 75%；当 $t_{8/5}$＝50 s（图 2c）和 $t_{8/5}$＝100 s（图 2d）时，奥氏体总的形态显现条块状，只是 $t_{8/5}$较长时，奥氏体组织呈块状聚在一起，而且由连续条状转变成粗块状，也有一部分呈尖锋状，两相边界明显，铁素体相内部析出奥氏体相明显增多，铁素体相比例分别约为65%和 55%。

结果表明，2205 双相不锈钢组织经过不同的热循环之后，即模拟焊接 HAZ 组织在不同的冷却条件下，组织的形态和分布与原来有了很大的区别。随着冷却时间的增加，奥氏体相由原来的拉长的条状，析出形态变得越来越粗大，析出越来越充分。同时从晶内成核析出的奥氏体变多，最后与晶界处析出的奥氏体互连在一起，两相的比例也有较大的变化。

在研究冷却速度对组织转变的影响时，对于常见的低碳钢和低合金钢，人们关注的是从800 ~ 500 ℃的冷却时间 $t_{8/5}$，这是因为800 ~ 500 ℃是奥氏体最不稳定的温度范围，$t_{8/5}$ 的长短将决定该材料最终的相变产物。而 2205 双相不锈钢属于高合金钢，其相图与一般的低碳钢和低合金钢 Fe — C 合金相图有很大的区别。

根据美国焊接研究委员会（WRC — 1992）采用的铬、镍当量比值所绘制的 Fe — Cr — Ni 三元截面相图（变种）（图 3）[6]。实际上所有双相不锈钢从液相凝固后首先都是完全的铁素体组织，这一组织一直保留至铁素体溶解度曲线的温度，只有在更低的温度下部分铁素体才转变成奥氏体，形成奥氏体铁素体双相组织。对 2205 双相不锈钢，从铁素体转变为奥氏体的温度范围是1 200 ~ 800 ℃，因此用 $t_{12/8}$ 作为参数研究 2205 双相不锈钢模拟 HAZ 的组织更为恰当。

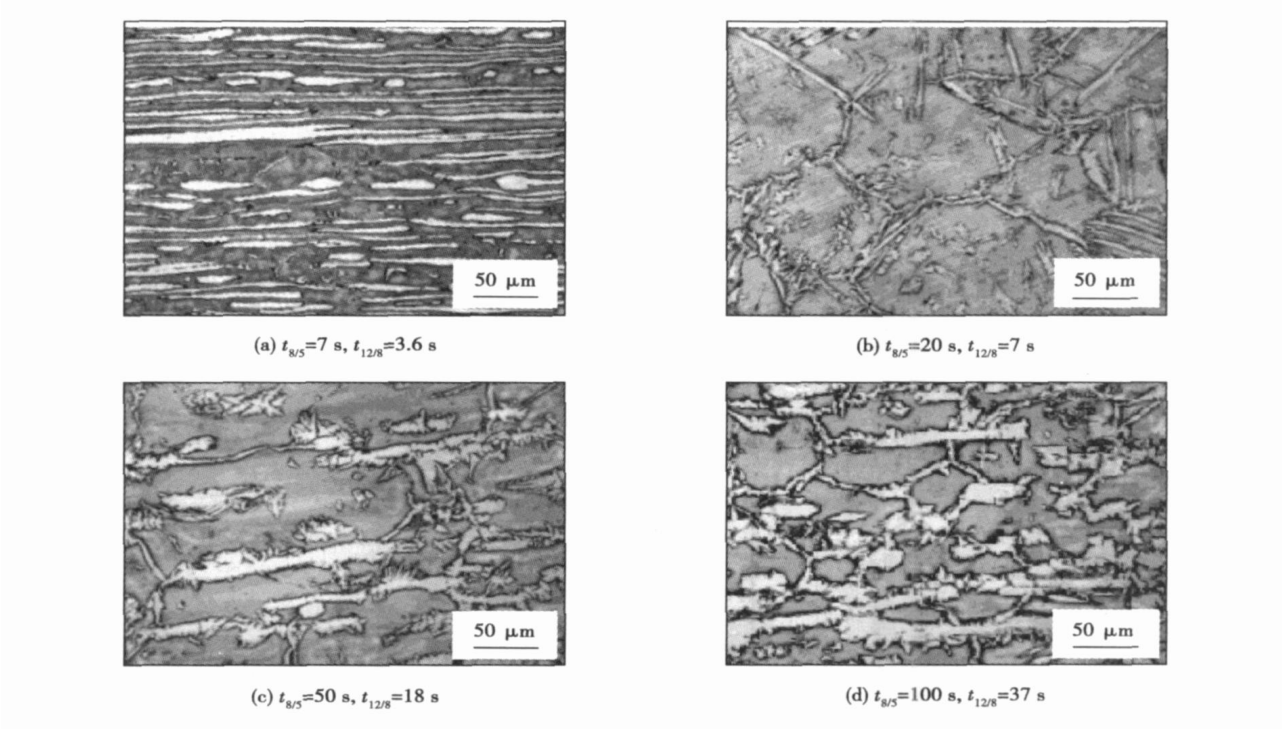

(a) $t_{8/5}$=7 s, $t_{12/8}$=3.6 s　(b) $t_{8/5}$=20 s, $t_{12/8}$=7 s

(c) $t_{8/5}$=50 s, $t_{12/8}$=18 s　(d) $t_{8/5}$=100 s, $t_{12/8}$=37 s

图 2　不同冷却时间模拟 HAZ 的组织

Fig. 2　Microstructure of simulation HAZ at diffidence cooling time

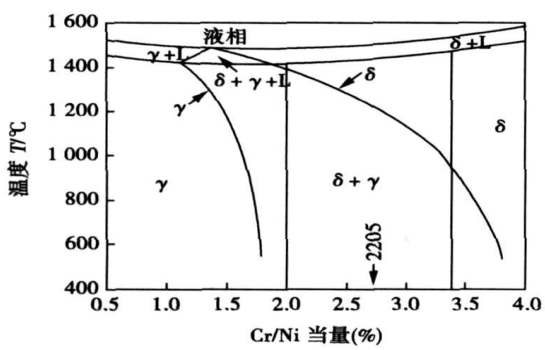

图 3　Fe—Cr—Ni 三元截面相图(变种)

Fig. 3　Fe—Cr—Ni three—component alloy phase diagram

为什么会出现上述假象呢？这是因为计算热循环曲线时，$t_{8/5}$在变化的同时，$t_{12/8}$也在同时变化，根据式(2)可以计算出对应 $t_{8/5}$为 7，20，50 和100 s时，$t_{12/8}$分别为 3.6，7，18 和37 s。

$$\frac{t_{8/5}}{t_{12/8}}=\frac{\dfrac{1}{(500-T_0)^2}-\dfrac{1}{(800-T_0)^2}}{\dfrac{1}{(800-T_0)^2}-\dfrac{1}{(1\ 200-T_0)^2}}。\qquad(2)$$

要搞清 $t_{8/5}$和 $t_{12/8}$这两个热循环参数各自对 2205 双相不锈钢模拟 HAZ 组织的影响，就应固定其中的一个参数，然后改变另一个参数，研究其显微组织特征。为了说明这点，进行了下述进一步的试验。

2.2　固定 $t_{12/8}$研究 $t_{8/5}$对 HAZ 组织转变的影响

固定 $t_{12/8}$=7 s，分别选取 $t_{8/5}$=7，20，50 和100 s，模拟 HAZ 的金相组织见图 4。组织形态都是在铁素体基体中析出长条状的奥氏体组织。在 $t_{8/5}$=7 s时两相相对来说分辨的比较清楚；当 $t_{8/5}$大于50 s后，室温组织的形态相似，基本上呈细长条状相互聚在一起，两相的边界已经变得有点模糊。铁素体相比例相差不大，均在 65％左右。

当固定 $t_{12/8}$，改变 $t_{8/5}$时，热循环参数 $t_{8/5}$对模拟 HAZ 组织形态和相比例影响不大，用 $t_{8/5}$研究 2205 双相不锈钢 HAZ 的组织转变行为是不恰当的。

2.3　固定 $t_{8/5}$研究 $t_{12/8}$对 HAZ 组织转变的影响

固定 $t_{8/5}$=20 s，分别选取 $t_{12/8}$=3.6，7，18 和37 s，模拟 HAZ 的金相组织形态见图 5。可以看出，几张照片金相组织形态差异较大，随着冷却时间 $t_{12/8}$的增加，奥氏体由原来的带状逐渐转变成树枝状或羽毛状，晶界和晶粒内部均析出奥氏体，相互交集在一起形成网状，两相的比例也有较大的差异。由此可见，$t_{12/8}$改变是引起 HAZ 组织变化的本质因素。

从图 3 的 FeCr—Ni 三元截面相图可知，对 2205 双相不锈钢，δ/γ 相界大约在1 150 ℃附近，从1 200～800 ℃是双相组织最不稳定的温度范围。模拟 HAZ 从峰值温度开始冷却时，特别是在 δ/γ 相界温度继续冷却时，组织开始发生转变，即发生铁素体到

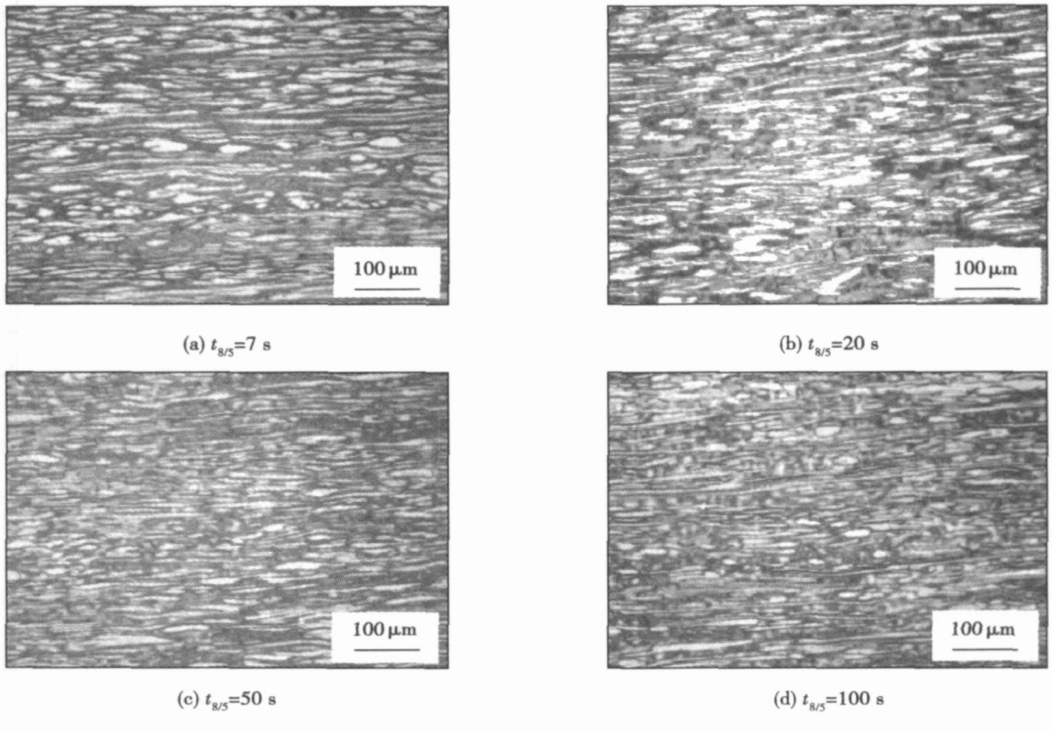

图 4 不同 $t_{8/5}$时 HAZ 金相组织($t_{12/8}$= 7 s)

Fig. 4 Microstructure of simulated HAZ at diffidence cooling time $t_{8/5}$

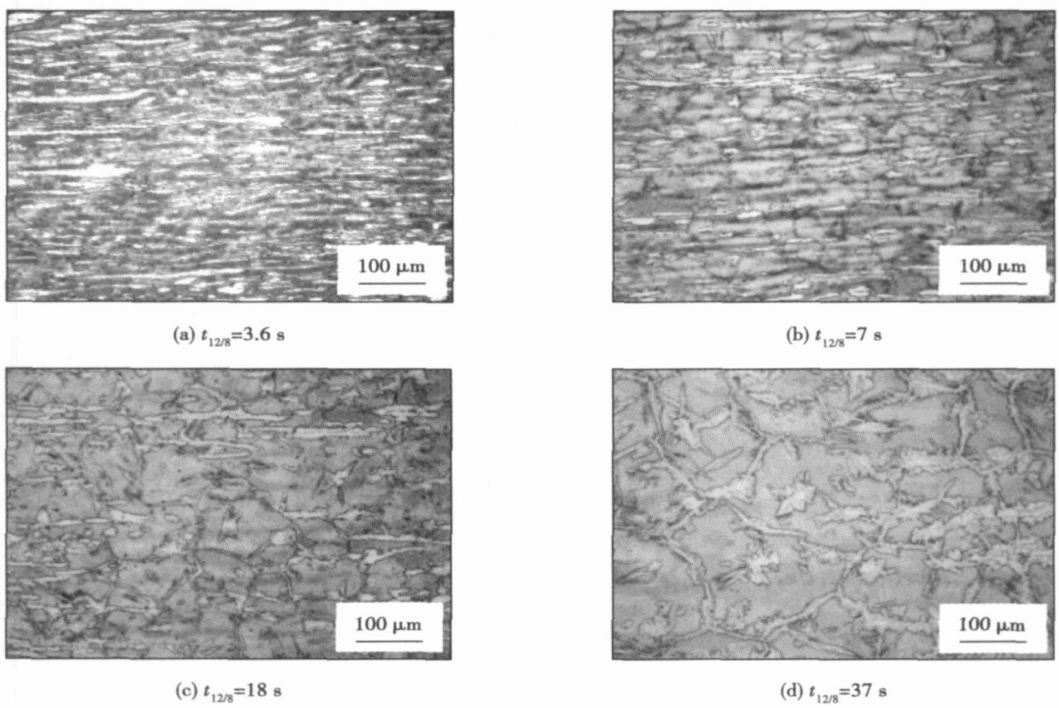

图 5 不同 $t_{12/8}$时 HAZ 金相组织($t_{8/5}$= 20 s)

Fig. 5 Microstructure of simulated HAZ at diffidence cooling time $t_{12/8}$

奥氏体的转变, 消除了原来的 δ/δ晶界, 形成了 δ/γ 相界。在冷却过程中随着 $t_{12/8}$时间的增加, 铁素体向奥氏体转变完成的程度增大。随着在 $t_{12/8}$时间进一步延长, 不但晶界处出现了奥氏体, 铁素体晶粒内部也通过形核向奥氏体转变。这样奥氏体的比例就越来越大, 并且随着时间的增加, 奥氏体逐渐长大连在一起形成网状结构。而在800 ~ 500 ℃的温度区间, 2205 双相不锈钢处在 δ+ γ 两相区, 此时组织中

的组织转变率远没有在 $t_{12/8}$ 温度区间来得大。因此，固定 $t_{8/5}$，改变 $t_{12/8}$，对 2205 双相不锈钢 HAZ 的组织形态和相比例的影响都比较大。$t_{12/8}$ 是影响其 HAZ 最终组织的本质因素，用它来研究对 2205 双相不锈钢 HAZ 组织的影响更为确切。

进一步分析 $t_{12/8}$ 对 HAZ 组织的影响，当冷却时间较短（$t_{12/8}$ = 3.6 s），由于热输入小，高温停留时间短，冷却速度很快，原来双相组织中的奥氏体只有部分转变成铁素体。当温度下降，$t_{12/8}$ 仅为3.6 s时，由于温度下降太快，铁素体向奥氏体的转变也很不充分，至室温时的组织形态与母材组织很相似，晶粒呈现条带状，铁素体所占比例与母材相比增大；在 $t_{12/8}$ = 7 s时，热输入增大，高温停留时间延长，原来双相组织中的奥氏体基本全部转变成铁素体，温度下降时，冷却时间相对短，只有铁素体晶粒边界析出了条块状的奥氏体，奥氏体相含量很少，铁素体相比例高（约为 80%）；$t_{12/8}$ 继续增加至18 s时，铁素体晶粒边界和晶粒内部均析出了羽毛状和条块状的奥氏体，并且互相交接在一起，奥氏体相含量与 $t_{12/8}$ = 7 s相比增大，铁素体相比例减少（约为 70%）；当 $t_{12/8}$ 增大到37 s时，这时在铁素体晶粒边界和晶粒内部析出的奥氏体组成网状结构，奥氏体相含量进一步增加，铁素体相比例进一步减少（约为 60%）。

图 6 是模拟 HAZ 组织（$t_{12/8}$ = 37 s，$t_{8/5}$ = 20 s）的透射电镜组织（TEM）照片。焊接是一个快速加热和冷却的过程，在这个过程中组织转变不平衡，经过热循环得到的 HAZ 组织的位错密度要远比母材组织里的位错密度大，铁素体组织的位错密度明显要比奥氏体组织大。在铁素体中，不同方位的位错线相互交叉固定在一起，能起到强化组织的作用。

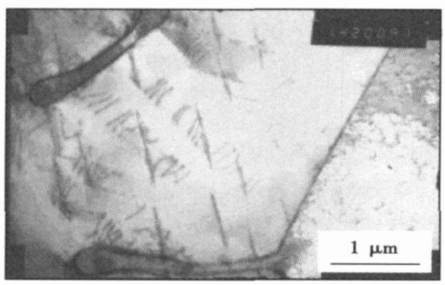

(a) 奥氏体内的位错

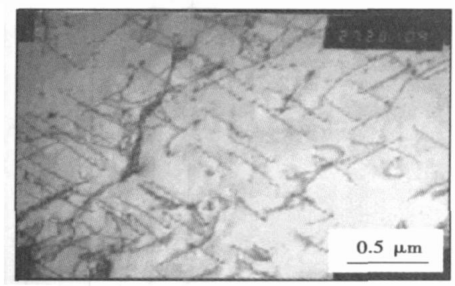

(b) 铁素体内的位错

图 6　模拟 HAZ 的 TEM 形貌

Fig. 6　TEM of simulated HAZ

3　结　　论

（1）固定 $t_{12/8}$，改变 $t_{8/5}$，2205 双相不锈钢模拟 HAZ 组织的形态和相比例相差不大，用 $t_{8/5}$ 作为参数研究这种材料 HAZ 组织转变行为是不恰当的。

（2）固定 $t_{8/5}$，改变 $t_{12/8}$，2205 双相不锈钢模拟 HAZ 的组织形态和相比例变化比较大。$t_{12/8}$ 是影响这种材料 HAZ 组织的本质因素，用它来研究对 2205 双相不锈钢 HAZ 组织的影响更为确切。

（3）冷却时间 $t_{12/8}$ 对 2205 双相不锈钢模拟 HAZ 组织的影响规律是随着 $t_{12/8}$ 的增加，奥氏体由原来的长条状逐渐变成树枝状，晶界和晶粒内部均析出奥氏体，相互交集在一起形成网状。铁素体的比例随着冷却时间 $t_{12/8}$ 的增加而缓慢下降。

（4）由于焊接快速加热和冷却的过程中组织转变不平衡，2205 双相不锈钢模拟 HAZ 组织中奥氏体和铁素体晶内比母材有更多的位错。

参考文献：

[1] Mats Liljas. The welding metallurgy of duplex steel[C] // International Duplex Stainless Steel Conference. China: Beijing, 2003, 25—39.

[2] Rouault P, Bonnet C. Make the duplex and super-duplex welding easier through metallurgical and practical simple recommendations[C] // International Duplex Stainless Steel Conference. China: Beijing, 2003, 95—97.

[3] Kordatos J D, Fourlaris G, Papadimitriou G. The effect of cooling rate on the mechanical and corrosion properties of UNS 31803 duplex stainless steel welds[J]. Scripta Mater, 2001, 44(3): 401—408.

[4] 牛济泰. 材料和热加工领域的物理模拟技术[M]. 北京：国防工业出版社，1999.

[5] 李尚周. 现代双相不锈钢焊接研究[J]. 华南理工大学学报，1996，24(8)：44—45.

[6] Lippold J C. Duplex stainless steels[C] // 4th International Duplex Stainless Steel Conference. UK: Glasgow, 1994: 115—118.

作者简介：熊庆人，女，1969 年出生，硕士，高级工程师。主要从事油气输送管材料的研究，获省部级科技进步二、三等奖共 5 项。发表论文 30 余篇。

Email：xiongqr@tgrc.org

hardness of laser cladding layer is within 600— 700 HV0. 2, and much higher than that of the matrix.

Key words: Ti($C_{0.3}N_{0.7}$) particle; TiN particle; in-situ reaction; laser cladding

Soldering technique of bronzes excavated from Jiuliandun tomb in Hubei province JIN Pujun[1], QIN Yin[1], HU Yali[2], WANG Changsui[3] (1. Department of Scientific and Technical History and Archaeology, University of Science and Technology of China, Hefei 230026, China; 2. Museum of Hubei Province, Wuhan 430060, China; 3. Graduate University, Chinese Academy of Sciences, Beijing 100049, China). p37— 40

Abstract: The oldering technique of Bronzes Excavated from Jiuliandun Tomb of Warring States in Chinese Hubei Province was investigated. According to naked-eye observation, it was concluded the welded splice used mortise-tenons, with smooth and crinkly soldered joint by thermal processing and that the pouring gates were designed at the bottom or the side wall. The solders were investigated using diffraction, X-ray fluorescence, scanning electron microscopy with energy dispersive X-ray detection and differential scanning calorimetry. Results show that solders were composed of Pb-Sn alloys with average mixture ration about Pb73 and Sn27 by XRF analysis, and the phase was as-cast microstructure observed by SEM, which indicated ancient people poured melting solder to connect different bronze parts, and the melting point of some solders existing in 180— 186 ℃ by DSC, which meant they had low work temperature and the aim to produce them just were used as bronze sacrificial ware.

Key words: solder; soldering history; Pb-Sn alloy; traditional craft

DSP based digital control system for GMAW-P WU Kaiyuan, HUANG Shisheng, LI Xinglin, KE Litao (School of Mechanical Engineering, South China University of Technology, Guangzhou 510640, China). p41— 44

Abstract: For the pulsed waveform modulation of GMAW-P (gas metal arc welding-pulsed arc), a novel DSP based digital control system for GMAW-P was presented, which was established based on 16-bit fixed point digital signal processor (DSP) TMS320LF2407A. By adopting the PWM generation modules integrated in DSP and selecting their reasonable working mode, the digital control of PWM signal was realized, so the high frequency inverter and low frequency pulsed waveform modulation of GMAW-P were realized, and the stability and reliability of control system were improved. The design of software to the control system was also discussed. Experimental results show that the developed digital control system has the ability to accomplish the excellent welding process and appearance of the weld is good, the merit of DSP based digital control system is fully demonstrated.

Key words: digital signal processor; gas metal arc welding-pulsed arc; digital control

Inverse design of spot welding nugget sizes and current parameters TANG Xinxin, SHAN Ping, LUO Zhen, YE Mao (College of Material Science and Engineering, Tianjin University, Tianjin 300072, China). p45— 48

Abstract: In order to made the physical dimension of nuggets meet the needs of mechanical properties, the inverse design of welded joint is introduced. Based on the mechanical properties, the qualified nugget sizes are determined. According to these, the numerical model is created. Through simulated calculation, the current parameters can be determined. Three kinds of regular shape nugget are used to research the relation between the mechanical properties and nugget sizes. Based on the stress graph, the diameter of nugget and the penetration rate varying with the tension stress, the nugget shapes are evaluated, the one which the stress distribution is the most evenly and the stress concentration is the most little is selected. According to the physical dimension of the nugget, the current parameter curve used for forming nugget is simulated by finite element simulate method.

Key words: resistant spot welding; nugget design; numerical simulation

Diode laser soldering for chip resistor component HAN Zongjie[1], XUE Songbai[1], ZHANG Xin[1], WANG Jianxin[1], FEI Xiaojian[1,2], YU Shenglin[1,3] (1. College of Materials Science and Technology, Nanjing University of Aeronautics and Astronautics, Nanjing 210016, China; 2. Guangzhou CSSC-Ocean-Gws Marine Engineering Co. Ltd., Guangzhou 510727, China; 3. The 14th Research Institute, China Electronics Technology Group Corporation, Nanjing 210013, China). p49— 52

Abstract: Diode soldering experiments of rectangular chip resistor components were carried out using Sn-Ag-Cu lead-free solder, the mechanical properties of the micro-joints were studied by STR-1000 micro-joints tester. The results indicate that as the laser soldering time is fixed, the shear force of chip resistor micro-joints becomes larger with the increase of laser output power, and the shear force is the largest at a optimum power. With the increase of laser soldering time, the optimum power decrease, and 1s is the best laser soldering time. Competitive experiments results show mechanical properties of chip resistor micro-joints soldered with laser soldering system is better than that of chip resistor micro-joints soldered with IR reflow soldering method.

Key words: rectangular chip resistor; Sn-Ag-Cu lead-free solder; diode laser soldering; mechanical properties of micro-joints

Transition behavior of welding HAZ microstructure of 2205 duplex stainless steel XIONG Qingren[1], HUO Chunyong[1], LI Weiwei[1], ZHANG Jianxun[2] (1. Tubular Goods Research Center of CNPC, Xi' an 710065, China; 2. School of Materials Science and Engineering, Xi' an Jiaotong University, Xi' an 710043, China). p53— 57

Abstract: Thermal simulation technology and modern material microstructure analysis method are adopted to research the effect of cooling time $t_{8/5}$ and $t_{12/8}$ on the simulated HAZ(heat-affected zone) microstructure transition in 2205 duplex stainless steel. The results indicate that keeping $t_{12/8}$ constant and changing $t_{8/5}$, the simulated HAZ microstructure and phase proportion almost keep same. So it is not suitable to this material to use $t_{8/5}$ as the parameter to investigate

the transition behavior of welding HAZ microstructure. When the cooling time $t_{8\delta}$ keeps constant and $t_{12\delta}$ is changed, the simulated HAZ microstructure and phase proportion vary largely. Therefore, $t_{12/8}$ is the essential factor to affect HAZ microstructure, and it is more suitable to use $t_{12/8}$ as the parameter to investigate the transition behavior of welding HAZ microstructure. The effect of the cooling time $t_{12\delta}$ on the simulated HAZ microstructure is, when $t_{12\delta}$ increases, austenite gradually transits to branch-like morphology from band-like distribution and appears at the boundary and inside the grain. On the other hand, the ferrite content decreases with the cooling time $t_{12/8}$ increasing. In this case, austenite and ferrite in the simulated HAZ microstructure of 2205 contain more dislocation than the base metal.

Key words: duplex stainless steel; heat-affected zone; microstructure; phase proportion

Microstructure and properties of copper alloy based nano composite for spot welding electrode DENG Jingquan[1,2], WU Yucheng[1], Zong Yue[3], WANG Wenfang[1], HUANG Xinmin[1], YU Fuwen[1] (1. School of Materials and Engineering, Hefei University of Technology, Hefei 230009, China; 2. School of Materials and Engineering, Zhejiang University, Hangzhou 310007, China; 3. Materials corporation, Hefei University of Technology, Hefei 230009, China). p58—60, 64

Abstract: Copper alloy-based composites were successfully prepared using PM method with mechanically alloyed powders for spot welding electrode(CuCrZr/AlN). Microstructure and properties were characterized using transmission electron microscope, scanning electron microscope etc. Their electrical conductivity, thermal conductivity and softening temperature were measured. Results show that with the increasing of the contents of AlN, the electrical and thermal conductivity both decrease while the softening temperature increases. When the content of AlN is 0.4wt%, its softening temperature reaches 900 ℃, while its electrical conductivity is about 45%IACS (international annealling copper standard) and its thermal conductivity is about 197 W/m·K. When the content of AlN is 0.2wt%, the composite has good comprehensive properties and is suitable for spot welding electrode.

Key words: Nano-composite CuCrZr/AlN; powder metallurgy; electrical conductivity; heat conductivity; softening temperature

Temperature field and stress field in arc sprayed coating of steel mold DONG Xiaoqiang, ZHANG Hongbing, LIU Yong, ZHANG Zhongli (School of Material Science and Engineering, Shenyang University of Technology, Shenyang 110023, China). p61—64

Abstract: In order to analyze the arc spraying deposition process during the mold manufacture the FEA simulation program was introduced to calculate the temperature field and stress field in the sprayed coating. The heat transfer from coating to substrate was taken into account when the mathematical model is put forward. The model is built through the micro-thickness increase of the coatings. The micro-thickness lamellas and method of element's birth or death are activated gradually to participate in the calculation. Movable boundary condition is used to simulate the practical deposition process adequately. On the basis of the calculation, the effect of the stress distribution on the coating unstable and the residual stress is analyzed.

Key words: arc spraying; mold; numerical simulation; temperature field; stress field

Analysis for Al—Fe intermetallic compounds layer of fusion-brazed joints between aluminium and zinc-coated steel by hybrid welding LEI Zhen, WANG Xuyou, WANG Weibo, LIN Shangyang (Harbin Welding Institute, Harbin 150080, China). p65—68

Abstract: The structure of Al—Fe intermetallic compounds in fusion-brazed joints between aluminium and zinc-coated steel was analyzed. Influence of welding energy input on the thickness of the Al-Fe intermetallic compounds layer was studied. And the influence of the thickness of the Al—Fe intermetallic compounds layer on the shear strength of joints was also studied. The results indicated that the intermetallic compounds layer was composed of Fe_3Al, $FeAl_2$, Fe_2Al_5 and $FeAl_3$, and these binary intermetallic compounds exhibited an enrichment of silicon near the weld metal side. The intermetallic compounds layer became more and more thicker along with the increasing of the welding energy input. But the effect of arc energy on the thickness of the layer was more remarkable than that of laser energy. A thinner or thicker Al—Fe intermetallic compounds layer could reduce the strength of the joints. When the the thickness of Al—Fe intermetallic compounds layer was within 1.5—4 μm, the influence of the layer on mechanical property of the joint was not significant.

Key words: laser; plusd metal inert-gas arc; hybrid welding; fusion-brazing joining; Al-Fe intermetallic compounds

Low-power YAG laser-MAG arc hybrid welding of stainless steel KANG Le[1,2], HUANG Ruisheng[1], LIU Liming[1], LIU Jinghe[2] (1. State Key Laboratory of Materials Modification, Dalian University of Technology, Dalian 116024, Liaoning, China; 2. School of Materials Science and Engineering, Changchun University of Science and Technology, Changchun 130022, China). p69—72

Abstract: This paper studied the low-power pulsed YAG laser-pulsed MAG arc hybrid welding of stainless steel based on the comparison between hybrid welding process and single pulsed MAG (metal active gas) arc welding. Compared with high-power laser-arc hybrid welding, the low-power pulsed YAG laser-pulsed MAG arc hybrid welding also had many same merits such as increasing penetration depth, improving welding speed and stabilization of welding process. The shape of the arc was changed in low-power pulsed YAG laser hybrid welding due to the input of low-power pulsed YAG laser. When the pulsed YAG laser acted on arc region, the attraction and contraction of the arc root in low-power pulsed YAG laser-pulsed MAG arc hybrid welding was prominent, and the energy absorption of MAG arc and pulsed YAG laser increased. The penetration depth in low-power pulsed YAG laser-pulsed MAG arc hybrid welding was 1.3 times of that in MAG welding when welding speed was same, and the welding speed increased 50 percent when the penetration depth was equal to that of MAG welding. The crystal grain of hybrid